Microbeam pull-in voltage topology optimization including material deposition constraint

E. Lemaire, V. Rochus, J.-C. Golinval, P. Duysinx
Aerospace and Mechanical Engineering Department, University of Liège, B52, Chemin des chevreuils 1, B4000 Liege Belgium

Abstract

Because of the strong coupling between mechanical and electrical phenomenon existing in electromechanical microdevices, some of them experience, above a given driving voltage, an unstable behavior called pull-in effect. The present paper investigates the application of topology optimization to electromechanical microdevices for the purpose of delaying the unstable behavior by maximizing their pull-in voltage. Within the framework of this preliminary study, the pull-in voltage maximization procedure is developed on the basis of electromechanical microbeams reinforcement topology design problem. The proposed sensitivity analysis requires only the knowledge of the microdevice pull-in state and of the first eigenmode of the tangent stiffness matrix. As the pull-in point research is a highly non-linear problem, the analysis is based on a monolithic finite element formulation combined with a normal flow algorithm (homotopy method). An application of the developed method is proposed and the result is compared to the one obtained using a linear compliance optimization. Moreover, as, the results provided by the developed method do not comply with manufacturing constraints, a deposition process constraint is added to the optimization problem and its effect on the final design is also tested.

Keywords : Topology optimization, electromechanical coupling, pull-in, manufacturing constraint

1 Introduction

The main idea underlying topology optimization is to avoid arbitrary decision on the connectivity or shape during the design stage of a structure. In consequence, the optimization problem is formulated as the research of the optimal material distribution maximizing a given objective function following some design constraints such as reliability constraints or manufacturing constraints. As proposed by seminal works [1, 2], the material distribution can be represented using an indicator function equal to '1' if material is present and '0' where it is void.

However, the topology optimization discrete form (0-1) is very difficult to solve because of its highly combinatorial nature. Usually, the highly combinatorial formulation is avoided by allowing the indicator function to vary continuously from 0 to 1. Contrary to the discrete version, the continuous problem can be solved using sensitivity analysis and efficient mathematical programming algorithms. Then, the indicator function can be considered as a density function representing the density of a porous material. Most often, the topology optimization problem is solved on the discretized version of the continuum mechanics problem using a finite element approximation. The density function is generally represented on this

mesh by attaching to each element a density design variable μ. Unfortunately, the resulting optimization problem is in general mathematically ill-posed and additional modifications are needed (see reference [3]) as inclusion of a perimeter constraint or filtering of the sensitivities which is presented in the following.

Next, considering a finite element mesh of the design domain, the properties of each element have to be estimated for continuous values of its density variable. This can first be performed on the basis of a microstructural approach using homogenization theory in order to ensure the physical meaning of the interpolation [1] or more simply by introducing a fictitious material model like the famous *SIMP* power law [2] which proposes to compute the Young Modulus E using a power law interpolation,

$$E = \mu^p E_0$$

where E_0 is the design material Young Modulus.

Currently, topology optimization has been applied as a systematic design tool to many problems involving one physics (see [4] for a review) like structural, electrical or magnetic problems (see Wang [5]). Conversely, the application of topology optimization to multi-physics problems is now under development. One of the earliest introductions of coupled behavior in topology optimization has been performed by Sigmund [6] for the optimal design of electrothermomechanical actuators. The problem considered by Sigmund includes three different physical fields, namely electric, thermal and mechanic. The analysis is based on a staggered scheme, which means that physical problems are solved successively. Since the coupling between physical problems is sequential, the solution can be reached without iteration. Given the electric input and output points, Sigmund's objective is to maximize the displacement in one direction of a target node. Moreover, Sigmund proposes extensions of the method to include large deformation assumptions, bi-material and multi-objective problems. More recently another improvement of the method has been proposed by Yin and Ananthasuresh [7]. They introduced a more accurate modeling of thermal convection and show under which conditions it can influence the final structure.

Topology optimization of electrostatically actuated microsystems has been originally proposed by Raulli and Maute [8]. These authors develop a topology optimization procedure for electrostatic force inverters. Their method is general since the optimization process can modify the topology of both physical domains at the price of a rather complicated staggered modeling. Nevertheless, original and interesting results are obtained. Later, Liu *et al.* [9] have proposed a topology optimization procedure aiming to maximize the mechanical compliance of electrostatically actuated devices. The method described by Liu *et al.* [9] makes use of SAND (Simultaneous Analysis ans Design) and of a level-set representation of the geometry. Moreover, topology optimization of electrostatic force inverters has also been studied very recently by Yoon and Sigmund [10] using the classical density distribution formulation and a monolithic analysis. Another interesting contribution in this field is the one from Abdalla *et al.* [11]. Using a simplified modeling based on a beam model, they have established a sizing method to adjust the thickness or width evolution along an electromechanical microbeam in order to maximize its pull-in voltage.

The present paper, synthesizing and deepening the authors' proceeding paper [12], extends the approach developed by Abdalla *et al.* using topology optimization combined with a monolithic electromechanical modeling provided by a multiphysic finite element approach implemented in OOFELIE [13]. The use of a coupled finite element analysis providing a field

description of the electrostatics allows a more precise modeling of the electrostatic domain as proposed by references [8, 10]. Moreover, the monolithic nature of our approach gives rise to a less complicated and more stable procedure while topology optimization leads to a more general optimization problem. As stated by the next section, pull-in effect is related to a non linear instability phenomenon and resembles buckling topology optimization problem which has been studied by several papers during last years (see for instance references [14, 15, 16, 17]). Pull-in appears in some electromechanical microdevices such as actuators and sensors and may damage them. Therefore, pull-in effect has to be kept away from the operating range of such microsystems. This could be done with the help of optimization by introducing a constraint over the pull-in voltage while optimizing a performance criterion such as the maximum displacement of an actuator, the capacitance of an RF switch or the stiffness of an accelerometer. However, in order to separate the difficulties of this kind of optimization problem, the present paper intends to investigate first the control of pull-in voltage in topology optimization. Therefore, the optimization problem that is here considered consists in maximizing the pull-in voltage of a microbeam with a restriction on the available material volume in order to obtain a non-trivial optimization problem.

However, as often in topology optimization, numerical results of our optimization procedure are too complicated to be produced using usual layer deposition manufacturing process. Recent work by Agrawal and Ananthasuresh [18] proposes an interesting reformulation of the optimization problem in order to handle layer deposition manufacturing constraint. In this paper, rather than reformulating the optimization problem, we investigate the possibility to consider the manufacturing constraint by introducing linear constraints in the optimization problem.

The paper begins with a brief description of the pull-in effect and its underlying physical phenomena. Next, we present the numerical methods used to compute the pull-in point and the sensitivities of the objective function. The knowledge of the pull-in configuration is required by sensitivity analysis. It is computed using a homotopy method coupled with the finite element modeling. The third section is dedicated to formulation of the optimization problem. The optimization problem and its hypotheses are posed and the implementation of a fabrication constraint is discussed. Before the conclusions, numerical applications of the developed method are proposed.

2 Electromechanical simulation and sensitivity evaluation

2.1 Pull-in phenomenon

Electrostatic actuation is a convenient and efficient way to produce forces in microelectromechanical devices. However, the non-linearity of the electrostatic force results in phenomena such as the pull-in effect. Pull-in effect is related to an unstable behavior of the actuator when the voltage exceeds an upper bound called the pull-in voltage. Physically speaking, this effect is very similar to non linear buckling occurring in mechanical structures. To explain the behavior of electrostatic actuators, let's consider the simplified device represented in figure 1. This capacitive system is made up of two parallels and rigid plates with the upper plate suspended by a linear spring of stiffness k and the lower plate fixed.

Considering that side effects are negligible, the electrostatic force resulting from the ap-

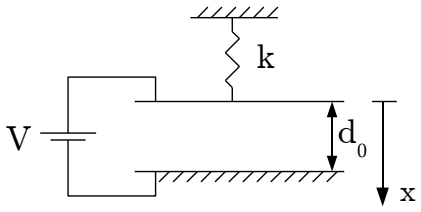

Figure 1: Simplified electromechanical actuator

plication of a voltage V between the plates can be written [19],

$$f_e = \frac{\varepsilon_0}{2}\frac{AV^2}{(d_0 - x)^2} \tag{1}$$

Where ε_0 denotes the permittivity of the media separating the plates (i.e. vacuum), A is the capacitor surface, d_0 the initial distance between the plates and x the displacement of the upper plate. Moreover, the restoring force from the spring is simply given by,

$$f_r = -kx$$

After applying the Newton's second law and a few manipulation of the resulting equation, we can obtain the following equilibrium equation giving the voltage as a function of the displacement.

$$V = \sqrt{\frac{2kx\,(d_0 - x)^2}{\varepsilon_0 A}} \tag{2}$$

Figure 2 plots the normalized equilibrium equation. We can see that this curve possesses a maximum in function of the voltage for $x = d_0/3$. This maximum corresponds to the pull-in voltage (V_{pi}) and no equilibrium position can be found for a greater voltage. By analogy with structural buckling, the pull-in voltage corresponds to a limit load. In practice, the application of an electric potential creates an electrostatic force which tends to bring the electrodes closer. However, as the displacement of the upper electrode increases, the electrostatic force increases also (see equation (1)). Consequently, at pull-in point, the spring cannot balance anymore the raising of the electrostatic force and the mobile electrode collapses toward the fixed one.

In addition, the pull-in point divides the equilibrium curve in two parts : a stable one (the left one) and an unstable one. This stability inversion can be checked by computing the effective stiffness (i.e. tangent stiffness) along the equilibrium path (x_e, V_e). The effective stiffness is simply obtained by computing the derivative of the total force $f = f_k + f_r$ applied to the mobile electrode with respect to its displacement.

$$k_{eff} = -\left.\frac{df}{dx}\right|_{x=x_e} = k - \frac{\varepsilon_0 A V_e^2}{(d_0 - x_e)^3} = k - \frac{2kx_e}{d_0 - x_e}$$

This expression shows that the tangent stiffness vanishes for $x_e = d_0/3$ resulting in unstable equilibrium position at pull-in point and for larger values of the displacement. This property will be used in the following to detect pull-in state.

The instability resulting from pull-in effect can be undesirable in microsystems. Indeed, this phenomenon may damage the device or even destruct it since even with a dielectric film it can be impossible to separate the electrodes from each other after pull-in in wet environment (see reference [20]). That's why this paper investigates the application of topology optimization to electromechanical problems in order to increase the pull-in voltage.

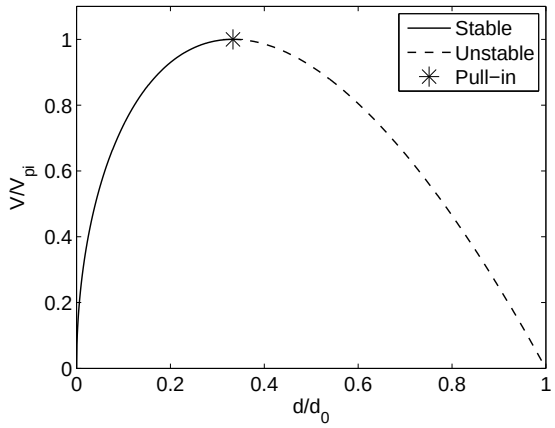

Figure 2: Equilibrium curve of the simplified actuator

2.2 Monolithic finite element formulation

The multiphysic modeling methods can be divided into two main groups. The first type of methods is the *staggered methods* (see Raulli *et al.* [8] for instance) where each physical field is solved separately and global coupled convergence is obtained using an iterative procedure. Staggered methods have the advantage to be simpler to implement since one can use existing computing codes to solve each physical field. However, staggered methods lack convergence in some difficult cases. For instance, in electromechanical simulations, staggered methods become unreliable when approaching pull-in. Therefore, it is difficult to compute accurately the pull-in point using this type of method.

Since precise knowledge of the pull-in configuration is needed by the optimization process, we choose here to use a method from the second set, namely monolithic methods. Contrary to staggered methods, monolithic methods consider the global problem and solve all physical fields at the same time. For instance, the monolithic finite element formulation developed by Rochus *et al.* [21] which is used here, allows computing a global tangent stiffness matrix including both mechanical and electrostatic problems.

In order to achieve a multiphysic coupling, Rochus *et al.* compute the internal work by integrating the Gibbs energy density on the computational domain Ω, resulting in,

$$W_{int} = \underbrace{\frac{1}{2}\int_{\Omega} \mathbf{S}^T\mathbf{T}\, d\Omega}_{mech.} - \underbrace{\frac{1}{2}\int_{\Omega(\mathbf{u})} \mathbf{D}^T\mathbf{E}\, d\Omega}_{elec.}$$

where the product between the strain tensor $\mathbf{S}$ and the stress tensor $\mathbf{T}$ corresponds to mechanical energy, while the product between $\mathbf{D}$ the dielectric displacement vector and $\mathbf{E}$ the electric field vector is equal to the electric energy contribution. Notice that the electrical term is integrated over the deformed domain $\Omega(\mathbf{u})$ which depends on the mechanical displacements $\mathbf{u}$.

By applying virtual work principle and discretizing the problem, Rochus *et al.* obtain a non linear equilibrium equation of the type,

$$\mathbf{r} = \mathbf{f}_{int} - \mathbf{f}_{ext} = \mathbf{0} \tag{3}$$

expressing that the difference between internal forces $\mathbf{f}_{int}$ and the external forces $\mathbf{f}_{ext}$ represented by the residual vector $\mathbf{r}$ has to be zero.

This non-linear equation is next linearized giving rise to equation (4) involving the global tangent stiffness matrix noted $\mathbf{K}_t$ following the notation of Géradin and Rixen [22]. This matrix can be partitioned in four blocks according to the physical nature of the related degrees of freedom. Denoting by $\mathbf{f}_m$ the mechanical forces and $\mathbf{q}_e$ the electrical charges, the linearized equilibrium equation can be written :

$$\underbrace{\begin{bmatrix} \mathbf{K}_{uu} + \mathbf{K}^*_{uu} & \mathbf{K}_{u\phi} \\ \mathbf{K}_{\phi u} & \mathbf{K}_{\phi\phi} \end{bmatrix}}_{\mathbf{K}_t} \underbrace{\begin{bmatrix} \Delta\mathbf{u} \\ \Delta\boldsymbol{\phi} \end{bmatrix}}_{\Delta\mathbf{q}} = \underbrace{\begin{bmatrix} \Delta\mathbf{f}_m \\ \Delta\mathbf{q}_e \end{bmatrix}}_{\Delta\mathbf{g}} \tag{4}$$

The first block $\mathbf{K}_{uu} + \mathbf{K}^*_{uu}$ links the mechanical displacements to the mechanical forces. The term $\mathbf{K}_{uu}$ corresponds to the classical mechanical stiffness while $\mathbf{K}^*_{uu}$ reflects the influence of the electrostatic force on the effective stiffness. Next, the two off-diagonal terms introduce a bilateral coupling between the electric and mechanical unknowns. Actually, $\mathbf{K}^*_{uu}$, $\mathbf{K}_{u\phi}$ and $\mathbf{K}_{\phi u}$ arise from the dependence of the electric energy toward mechanical displacements. Finally, $\mathbf{K}_{\phi\phi}$ simply corresponds to the purely electrostatic problem stiffness matrix.

On the basis of the global matrix it is possible to use homotopy methods (which are also called sometimes numeric continuation methods) to follow the equilibrium curve and to pass over the pull-in point. Among suited homotopy method we can mention the *normal flow* [23] and *Riks-Crisfield* [24] algorithms. The high reliability of these procedures allows localizing accurately the pull-in point.

2.3 Normal flow algorithm

As stated in the next section, the optimization process relies on the precise knowledge of the pull-in configuration. They can be computed by following the equilibrium curve starting from the rest position. As shown by Rochus *et al.* in reference [21], the classical Newton-Raphson scheme cannot be used for the pull-in point search problem. Indeed, given a fixed load (the electric potential in the present case) Newton-Raphson researches the corresponding equilibrium position. Therefore, if the voltage is chosen higher than the pull-in voltage, the algorithm will never be able to converge since no equilibrium position exists for this voltage. Moreover, the poor numerical conditioning of the problem around the pull-in point makes Newton-Raphson highly unstable when approaching this point. However, Rochus shows also that homotopy methods like Riks-Crisfield are suitable to compute pull-in configuration accurately.

Homotopy methods are mainly based on Newton-Raphson procedure and they also use alternately a tangent prediction and a correction phase. The difference with Newton-Raphson lies in the addition of a load variable λ to the unknowns of the problem. In the framework of our electromechanical problem, the applied electric potential V is chosen as load variable. This extra variable allows the correction process to adjust the load level applied on the system. Obviously, determining the additional variable requires the introduction of a new equation. Particular homotopy methods are characterized by the additional constraint chosen. In this paper, we use the normal flow method (see references [11, 23]) which imposes that the correction has to be perpendicular to the set of curves defined by perturbing the equilibrium equation (3),

$$\mathbf{r}\left(\mathbf{q}, V\right) = \boldsymbol{\delta}$$

where $\boldsymbol{\delta}$ is any perturbation vector. This set of curves is called the *Davidenko flow*. The principle of a normal flow iteration method is illustrated in figure 3 for a one-degree-of-freedom system. We can see the prediction step starting from point n on the equilibrium curve (continuous line) and the correction phase (points l, $l+1$, ...) normal to the *Davidenko flow* (dashed) leading to a new converged point $n+1$.

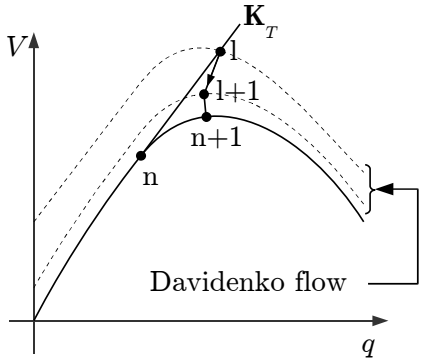

Figure 3: Normal flow method

Mathematically, the normal flow correction process is based on the linearized expression of the residual $\mathbf{r}$ around one given point $(\mathbf{q}_l, V_l)$,

$$\mathbf{r}\left(\mathbf{q}_{l+1}, V_{l+1}\right) = \mathbf{r}\left(\mathbf{q}_l + \Delta\mathbf{q}, V_l + \Delta V\right) \simeq \underbrace{\mathbf{r}\left(\mathbf{q}_l, V_l\right)}_{\mathbf{r}_l} + \underbrace{\frac{\partial \mathbf{r}}{\partial \mathbf{q}}}_{\mathbf{K}_t} \Delta\mathbf{q} + \frac{\partial \mathbf{r}}{\partial V}\Delta V \tag{5}$$

The problems considered in this paper include no external forces depending on the generalized displacements. Therefore, $\mathbf{r}$ is function of $\mathbf{q}$ solely through the internal forces. This is why we have from equation (3),

$$\frac{\partial \mathbf{r}}{\partial \mathbf{q}} = \frac{\partial \mathbf{f}_{int}}{\partial \mathbf{q}} = \mathbf{K}_t \tag{6}$$

where $\mathbf{K}_t$ stands for the tangent stiffness matrix. Moreover, since the applied voltage V corresponds to imposed degrees of freedom, the derivative of $\mathbf{r}$ with respect to V can be written,

$$\frac{\partial \mathbf{r}}{\partial V} = \frac{\partial \mathbf{r}}{\partial \mathbf{q}^i}\frac{\partial \mathbf{q}^i}{\partial V} = \mathbf{K}_t^{f,i}\frac{\partial \mathbf{q}^i}{\partial V} \tag{7}$$

where $\mathbf{K}_t^{f,i}$ corresponds to the partition of the full tangent stiffness matrix linking free and imposed degrees of freedom and $\mathbf{q}^i$ stands for the vector of imposed degrees of freedom. The components of the vector $\partial \mathbf{q}^i / \partial V$ take a constant value (generally 1) if the degree of freedom is electric and imposed and value 0 otherwise.

Since the objective is to find $\Delta\mathbf{q}$ and ΔV such that $\mathbf{r}$ vanishes, equation (5) becomes when cast under matrix form

$$\underbrace{\left[\begin{array}{cc} \mathbf{K}_t & \frac{\partial \mathbf{r}}{\partial V} \end{array}\right]}_{D\mathbf{r}} \underbrace{\left[\begin{array}{c} \Delta\mathbf{q} \\ \Delta V \end{array}\right]}_{\Delta\mathbf{c}} = -\mathbf{r}_l \tag{8}$$

To ensure perpendicularity between the correction vector $\Delta\mathbf{c}$ and the Davidenko flow, one simply imposes that $\mathbf{w} \cdot \Delta\mathbf{c} = 0$ where $\mathbf{w}$ is the tangent to the Davidenko flow computed by extracting the kernel of $D\mathbf{r}$. Next, to introduce the perpendicularity constraint in system of equations (8), $\mathbf{w}$ is partitioned into a vector $d\mathbf{q}/ds$ and a scalar dV/ds, s being a curvilinear abscissa,

$$\begin{bmatrix} \mathbf{K}_t & \frac{\partial \mathbf{r}}{\partial V} \\ \frac{d\mathbf{q}}{ds} & \frac{dV}{ds} \end{bmatrix} \cdot \begin{bmatrix} \Delta\mathbf{q} \\ \Delta V \end{bmatrix} = \begin{bmatrix} -\mathbf{r}_l \\ 0 \end{bmatrix} \tag{9}$$

In our multi-physic problem, the vector of unknowns $\Delta\mathbf{c}$ includes both voltages and mechanical displacements. Moreover, in MEMS context, the order of magnitude difference between electric and mechanical unknowns is generally large (voltage of at least 1 V and displacement about 1 μm). Therefore, in practice, to achieve a stable computation, it is necessary to normalize the problem in such a way that all components of vector $\mathbf{c}$ are of the same order of magnitude. As a result, the load variable is changed to $V/\hat{V}$ where $\hat{V}$ is the normalization factor of the electric potentials.

2.4 Pull-in voltage sensitivity analysis

Considering the finite element formulation presented above, the conditions governing pull-in state can be obtained. First of all, the pull-in point is located on the equilibrium curve and therefore, the equilibrium equation (3) has to be verified. Secondly, we have seen for the single degree of freedom system that the tangent stiffness vanishes at pull-in point. For multiple degrees of freedom, this means that pull-in occurs when the tangent stiffness matrix becomes singular. Sum of all, pull-in conditions are similar to the one obtained in reference [17] for non-linear buckling and can be written,

$$\begin{cases} \mathbf{r}\left(\mathbf{q}, V\right) = \mathbf{0} \\ \det\left(\mathbf{K}_t\left(\mathbf{q}, V\right)\right) = 0 \end{cases}$$

Using these equations, it is possible to obtain an analytical expression of the pull-in voltage sensitivities with respect to the topology optimization design variables namely, the pseudo-densities $\boldsymbol{\mu}$. This expression is highly useful since it provides an efficient way to compute numerically consistent sensitivities. The sensitivities equation can be established starting from the equilibrium equation by using a similar approach to references [11, 17]. At first, the equilibrium equation (3) is derived with respect to the pseudo-density μ_i,

$$\frac{\partial}{\partial \mu_i}\left(\mathbf{r}\left(\mathbf{q}, V\right) = \mathbf{0}\right) \quad \Leftrightarrow \quad \frac{\partial \mathbf{r}}{\partial \mu_i} + \frac{\partial \mathbf{r}}{\partial \mathbf{q}}\frac{\partial \mathbf{q}}{\partial \mu_i} + \frac{\partial \mathbf{r}}{\partial V}\frac{\partial V}{\partial \mu_i} = \mathbf{0}$$

As the equilibrium equation is considered at pull-in point, both derivatives of V and $\mathbf{q}$ with respect to μ_i have to be conserved in the equation. Indeed, the modification of the structure will not only result in a perturbation of the pull-in voltage, but as illustrated in figure 4, it will also change the deformation state at pull-in. Adopting the notations of last section and using equations (6) and (7) the derivative of the residual forces can then be expressed as,

$$\frac{\partial \mathbf{r}}{\partial \mu_i} + \mathbf{K}_t\frac{\partial \mathbf{q}}{\partial \mu_i} + \mathbf{K}_t^{f,i}\frac{\partial \mathbf{q}^i}{\partial V}\frac{\partial V}{\partial \mu_i} = \mathbf{0}$$

In the considered optimization problem, the perturbation of a pseudo-density μ_i can only modify directly the mechanical domain (see section 3.1). In addition, there is no external

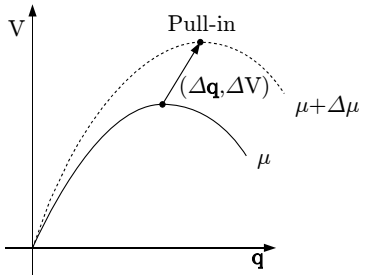

Figure 4: Evolution of the pull-in curve resulting from a perturbation of μ_i.

force in the considered problems. Therefore, the variation of $\mathbf{r}$ resulting from a density perturbation comes solely from the mechanical contribution to the internal forces $\mathbf{f}_{int}$. Since we consider small displacements, we have finally,

$$\frac{\partial \mathbf{S}}{\partial \mu_i}\mathbf{q} + \mathbf{K}_t \frac{\partial \mathbf{q}}{\partial \mu_i} + \underbrace{\mathbf{K}_t^{f,i}\frac{\partial \mathbf{q}^i}{\partial V}}_{\partial \mathbf{r}/\partial V}\frac{\partial V}{\partial \mu_i} = \mathbf{0} \tag{10}$$

if $\mathbf{S}$ denotes linear stiffness matrix of the mechanical part of the system. This last equation resembles the one obtained by Abdalla *et al.*, while the last term is different. However, the physical meaning of this term remains the same since $\partial \mathbf{r}/\partial V$ also represents the derivative of the electrical forces with respect to the load variable (V). Indeed, an increment of voltage will only affect the electric energy. Therefore, $\partial \mathbf{r}/\partial V$ has a purely electrical origin and in fact we can write

$$\frac{\partial \mathbf{r}}{\partial V} = \mathbf{K}_t^{f,i}\frac{\partial \mathbf{q}^i}{\partial V} = -\frac{\partial \mathbf{f}_{elec}}{\partial V}$$

where $\mathbf{f}_{elec}$ represents the electric contribution to the internal forces. Please note that this vector contains both mechanical electrostatic forces and electric charges.

Since the tangent stiffness matrix $\mathbf{K}_t$ is singular at pull-in point, the product of this matrix with its first eigenvector $\mathbf{p}$ is equal to zero (i.e. $\mathbf{K}_t\mathbf{p} = \mathbf{0}$). Moreover, we consider that $\mathbf{p}$ is normalized such that the following equation is verified,

$$\mathbf{p}^T\mathbf{K}_t^{f,i}\frac{\partial \mathbf{q}^i}{\partial V} = -1$$

Consequently, the left multiplication by $\mathbf{p}^T$ of equation (10) at pull-in point gives the following expression.

$$\frac{\partial V_{pi}}{\partial \mu_i} = \mathbf{p}^T\frac{\partial \mathbf{S}}{\partial \mu_i}\mathbf{q} \tag{11}$$

The last equation corresponds to the sensitivity of the pull-in voltage with respect to the design variable μ_i. This expression can be evaluated knowing the pull-in configuration of the current structure $\mathbf{q}$ and the corresponding $\mathbf{K}_t$ eigenmode $\mathbf{p}$. Therefore, the computation of the sensitivities with respect to every variable requires solely one pull-in point search. The sensitivities provided by equation (11) have been compared with respect to finite differences in order to validate the implementation of the analysis and sensitivity computation procedures.

However, particular care has to be taken when using this sensitivity expression. Indeed, if $\mathbf{p}$, the first eigenmode of $\mathbf{K}_t$ corresponds to a multiple eigenvalue, the optimization problem

is then non differentiable. This problem has already been treated for dynamic eigenvalues optimization where non differentiability is addressed by using a min-max scheme in order to include several eigenvalues in the optimization problem [25]. However, in the present paper, the optimization problem applications under consideration are unlikely to present multiple eigenvalues and therefore we did not had to use a min-max formulation.

2.5 Analysis implementation

Using the tangent stiffness matrix provided by the monolithic finite element formulation, the normal flow algorithm is able to follow the equilibrium curve even along its unstable side. Additional elements are added to the normal flow algorithm in order to integrate it into the optimization procedure as shown by the optimization loop flowchart given in figure 5.

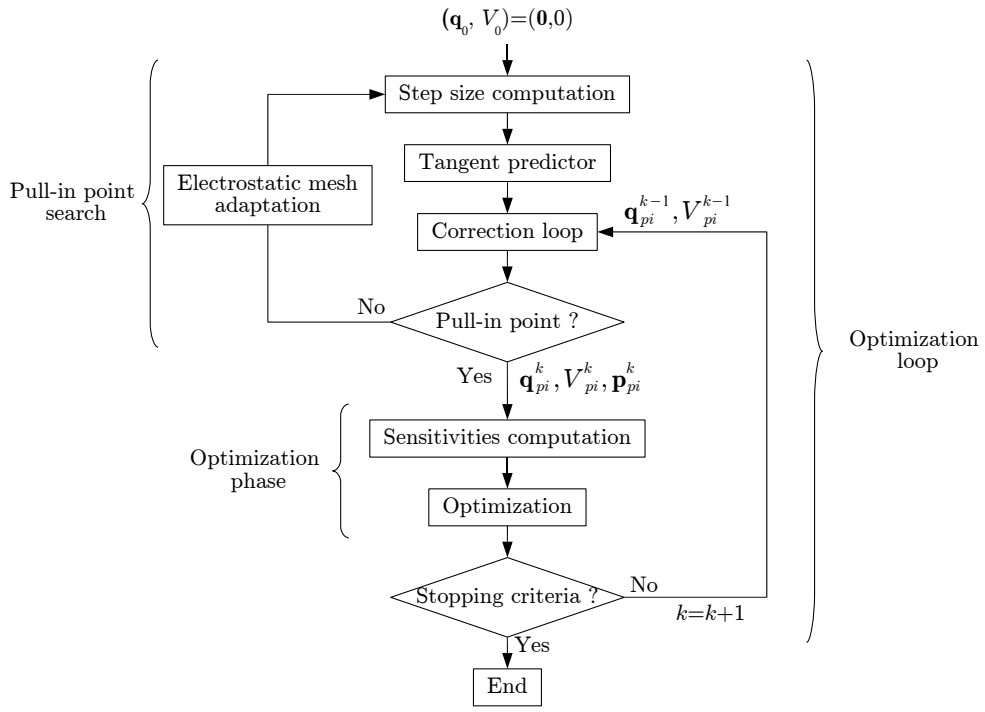

Figure 5: Flowchart of the optimization procedure

First of all, in order to locate the pull-in point accurately, the step size (equal to the norm of the predictor) is computed using a regula falsi based on $V' = dV/ds$ which zeroes at pull-in since V is maximal at this point. This derivative has the advantage to be computed systematically during the correction process through the evaluation of the $D\mathbf{r}$ kernel. Therefore as shown in figure 6, the equilibrium curve is firstly followed with a constant step size while monitoring the sign of dV/ds. When this sign changes, a regula falsi procedure is activated to compute the new steps size in order to zero dV/ds.

Secondly, a mesh displacement procedure has to be added for the electrostatic mesh. Indeed, mesh nodes of the electrostatic part of the domain do not have mechanical degrees of freedom and remain fixed while the mechanical nodes are moving. By the way, some electrostatic elements located at the boundary between the two physical domains may become

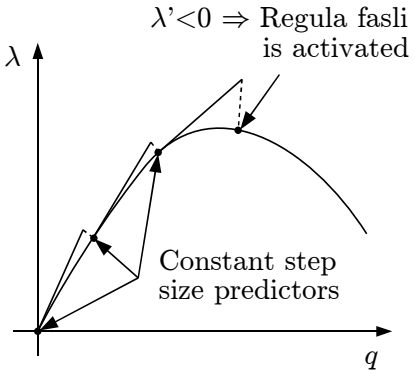

Figure 6: Pull-in search principle

strongly distorted. As proposed by Rochus *et al.* in reference [21], the electrostatic mesh is deformed at each pull-in search iteration to avoid numerical instabilities by solving a fictitious mechanical problem on the electrostatic domain.

Once the pull-in search has converged, the current pull-in voltage V_{pi}^k, the deformation state at pull-in $\mathbf{q}_{pi}^k$ and the first eigenmode of the tangent stiffness matrix $\mathbf{p}_{pi}^k$ are transmitted to the optimization module (k being the index of the optimization loop). Indeed, we have seen previously that the sensitivities evaluation makes use of the first eigenmode of the tangent stiffness matrix $\mathbf{K}_t$ at pull-in point. However, since this matrix is singular at pull-in, its first eigenmode corresponds to its kernel. Because dV/ds zeroes at pull-in the kernel of $\mathbf{K}_t$ and consequently its first eigenmode are included into the kernel of $D\mathbf{r}$ (see section 2.3). Therefore, the sensitivity analysis does not require any additional modal analysis.

Another asset of the normal flow method is that the correction procedure can be easily started from any point. Thus, as proposed in reference [17], the analysis computational cost can be reduced by using as a first guess the last structure pull-in configuration $(\mathbf{q}_{pi}^{k-1}, V_{pi}^{k-1})$ as shown in figure 5 rather than restarting from the rest position. This explains why the normal flow algorithm has been selected for this study instead of Riks-Crisfield as proposed by Rochus *et al.* in reference [21]. Indeed, Riks-Crisfield correction process is forced to follow a circle centered on the last converged point (i.e. the starting point of the current iteration). Therefore, Riks-Crisfield may fail while started from a non-equilibrium point as there may be no intersection between the curve and the constraint circle if its radius is chosen too small. Conversely, by only imposing perpendicularity of the increments to the Davidenko flow, the normal flow avoids this problem.

3 Optimization problem

3.1 Topology optimization of pull-in voltage

The application of topology optimization to problems involving one physical field has been investigated for a few years. However, the use of topology optimization for multiphysic problems is not always straightforward as shown by Raulli in Ref. [8] in the case of electromechanical coupling. The main difficulty of electromechanical optimization problems arises from the location of the electrostatic forces application point. These forces should normally be applied

at the boundary between void and solid. However, with topology optimization this boundary is usually unclear since there is often a smooth transition between void and solid.

In the scope of this preliminary study, we choose to circumvent this difficulty by considering a reinforcement problem where the electrical and mechanical domains are separated by a non optimizable layer of perfectly conducting material. The figure 7 represents the optimization problem considered in this perspective. In this figure, the non-optimizable layer, drawn in dark gray, corresponds to the mobile electrode. The electric domain lies under this electrode in white, while the optimization domain is located above. Therefore, the optimization domain is purely mechanical since it is insulated from electrical field by a non design perfectly conducting electrode. Moreover, the mobile electrode can be seen as an unalterable interface between mechanical and electrical domain.

Actually, the optimization problem consists in designing an optimal suspension to the mobile electrode. The design material is an elastic-linear material under small strains assumption. However, the studied problem is still multiphysic and strongly non-linear since the interaction between mechanical and electric phenomena remains.

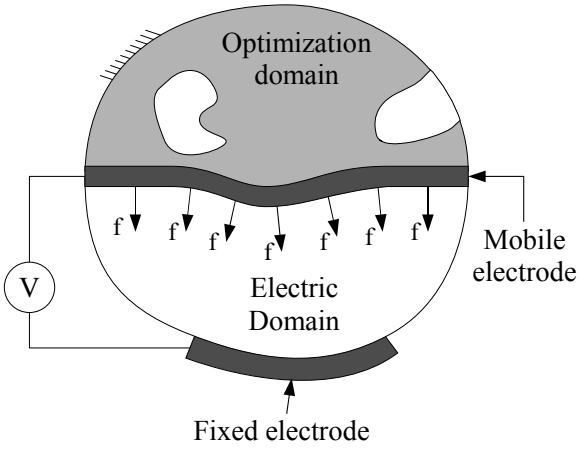

Figure 7: Schematic view of the considered optimization problem

The design problem that is considered here is to maximize the pull-in voltage of an electromechanical device with a bound on the available volume of material. This can be mathematically stated as follow,

$$\max_{\boldsymbol{\mu}} V_{pi}\left(\boldsymbol{\mu}\right)$$
$$s.t. \begin{cases} \sum_i \mu_i v_i \leqslant \overline{v} \\ \mu_{min} \leqslant \mu_i \leqslant 1 \quad \forall i \end{cases}$$

where $\boldsymbol{\mu}$ represents the vector of unknowns element density variables, $\overline{v}$ the upper bound on available material volume, v_i the i^{th} element volume and μ_{min} the lower bound on the unknowns.

The present study is based on the classical implementation of the topology optimization problems using continuous variables proposed by Bendsøe [2]. The mechanical properties are interpolated according to the *SIMP* power law [2], resulting for an element of density μ in a Young Modulus E equal to

$$E = \mu^p E_0$$

where E_0 is the original Young Modulus of the design material and p is the penalty parameter. However, this formulation leads to a mathematically ill-posed optimization problem as highlighted by references [26, 27, 3]. To remedy this difficulty, we choose to use a sensitivity filtering procedure to regularize the optimization problem. This heuristic method, originally proposed by Sigmund [27], replaces the sensitivity of each element by a weighted average of the original sensitivities existing in its neighborhood.

Thanks to the sensitivity analysis described in section 2.4, it is possible to use mathematical programming optimization algorithms based on a sequential convex programming approach (see reference [28]). These optimizers have proved to be very efficient even when handling a large number of design variables as it is the case in topology optimization. Several programs have been developed following this concept as for instance *MMA* by Svanberg [29] and *CONLIN* by Fleury [30] the latter being used in the present paper. Nevertheless, because of the monotonic character of *CONLIN* an adaptive move limit strategy similar to the one proposed by Svanberg in reference [29] has been implemented in order to prevent oscillations of the optimization process occurring in some applications. The goal of the adaptation procedure is to decrease the maximum allowed variation of a variable which oscillates in order to stabilize the optimization process.

The stopping criterion of the optimization loop is based on the greatest variation of the design variables between two successive iterations. By the way, we consider that the optimization process has reached convergence when the design variable greatest absolute modification drops under 0.01.

3.2 Fabrication constraint

The topology optimization procedure described above can already be applied and provides good results as this will be shown in the first example of the applications section. However, resulting topologies contain closed holes and therefore are unsuited to the classical microfabrication techniques since MEMS are usually produced using a deposition process of thin layers of material. Consequently, a manufacturing constraint inspired from the one used in topology optimization of molded parts (see references [31, 32]) has been implemented. To prevent the optimizer to close an upward opened hole, we simply impose that the pseudo-densities have to decrease monotonously while going upward in every column of the finite element mesh. This constraint can be stated mathematically as follows considering one column of elements

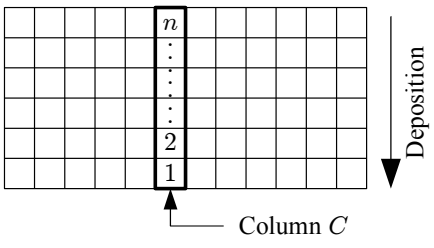

Figure 8: Pseudo-densities numbering in the expression of manufacturing constraint (12)

where pseudo-densities are numbered according to figure 8,

$$\begin{cases} 1 & \geqslant & \mu_1 & \geqslant & \mu_2 & & \\ & & \vdots & & & & \\ \mu_{i-1} & \geqslant & \mu_i & \geqslant & \mu_{i+1} & \text{if} & 2 \leqslant i \leqslant n-1 \\ & & \vdots & & & & \\ \mu_{n-1} & \geqslant & \mu_n & \geqslant & \mu_{min} & & \end{cases} \tag{12}$$

Conversely to the method proposed by Agrawal and Ananthasuresh [18], this constraint does not allow considering multi-material processes. However, it avoids a reformulation of the optimization problem and gives rises to optimal structures free of closed cavities.

The implementation of this kind of constraints results in a number of linear constraints approximately equal to the number of design variables. When using dual optimizer like *CONLIN*, such a huge number of linear constraints is a high penalty since it gives rise to as much dual variables and reduces the optimizer efficiency.

To reduce the amount of dual variables, it is possible to convert the linear constraints into side constraints, namely,

$$\underline{\mu_i^k} \leqslant \mu_i^k \leqslant \overline{\mu_i^k} \quad \forall i \in \{1, 2, \ldots, n\} \tag{13}$$

where the lower bound $\underline{\mu_i^k}$ and the upper bound $\overline{\mu_i^k}$ are constants given to the optimizer before iteration k. Therefore, in order to prevent the optimizer from violating (12) and to avoid a flipping of the variables, the side constraints expression has to be more conservative than the original linear constraints. We choose to compute the bounds as follow,

$$\underline{\mu_i^k} = \begin{cases} \mu_i^{k-1} - \frac{\mu_i^{k-1} - \mu_{i+1}^{k-1}}{2} & \text{if} \quad 1 \leqslant i \leqslant n-1 \\ \mu_{min} & \text{if} \quad i = n \end{cases}$$

$$\overline{\mu_i^k} = \begin{cases} 1 & \text{if} \quad i = 1 \\ \mu_i^{k-1} + \frac{\mu_{i-1}^{k-1} - \mu_i^{k-1}}{2} & \text{if} \quad 2 \leqslant i \leqslant n \end{cases}$$

Then, the drawback of this zero order approximation of (12) is a strong reduction of the admissible design space. As a result, the variables modification by the optimizer becomes smaller and the number of global iterations (i.e. analysis and optimization) to reach optimum will increase drastically. Nevertheless, with fewer dual variables, it is now possible to solve the optimization problem.

4 Applications

This section proposes numerical examples in order to illustrate the efficiency of the developed method as well as the usefulness of the manufacturing constraint.

4.1 Clamped-clamped beam topology optimization

The first application example of the developed method consists in the design of an optimal reinforcement suspension for a clamped-clamped microbeam. The problem is schematically represented with its dimensions in figure 9. As we can see, every side nodes of the prescribed

beam (represented in black) and of the optimization domain (drawn in light grey) are clamped. The non design electrode covers the whole length of the domain. The design material is an isotropic quartz possessing an elastic modulus $E = 86.79$ GPa and a Poisson's ratio $\nu = 0.17$. The available quartz volume is limited to 40 % of the design domain volume. The gap between the fixed and the mobile electrode is filled by air whose permittivity is $\varepsilon = 8.84 \cdot 10^{-12}$ F/m.

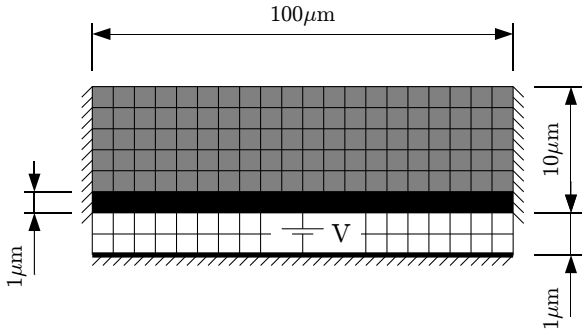

Figure 9: Dimensions and boundary conditions for the clamped-clamped beam

Of course, inasmuch as the problem is symmetric, we can model only one half of the device. The half design domain is discretized using a mesh of 100 by 18 nodes resulting in $99 \times 17 = 1683$ elements. The minimal density μ_{min} is set to 0.01. Moreover, numerical experiments have shown that this application provides better results when the penalty parameter evolves according to a continuation technique as described by Sigmund [33]. Therefore, we have adopted the following evolution scheme; starting from $p = 1$ the penalty is incremented of 1.0 each time the optimization problem has reached convergence according to stopping criterion. The process continues up to $p = 4$. Finally, a sensitivity filter is applied with a radius equal to 1.2 times the element greatest dimension.

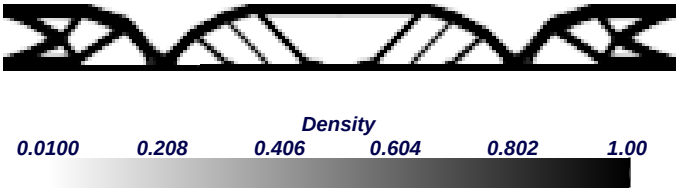

Figure 10: Final topology while optimizing pull-in voltage

The resulting topology is presented in figure 10. This structure contains very few intermediate density elements and presents a clearly defined bridge shape which is classic in topology optimization. The adaptive move limit strategy has been used to prevent small oscillations occurring at the end of the optimization process. The complete optimization process requires 269 iterations and the evolution of the pull-in voltage during the iterative process is plotted in figure 11. The three drops of the objective function shown by the figure are related to the penalty parameters increments of the SIMP law. Also, this figure shows that the optimizer increases the pull-in voltage from 727 V to 755 V. However, since the initial pull-in voltage is computed with $p = 1$ and the final one with $p = 4$, it does not actually make sense to

compare them. With $p = 4$ the pull-in voltage of the initial structure is equal to 258 V which leads to an increase of 193% during the optimization process.

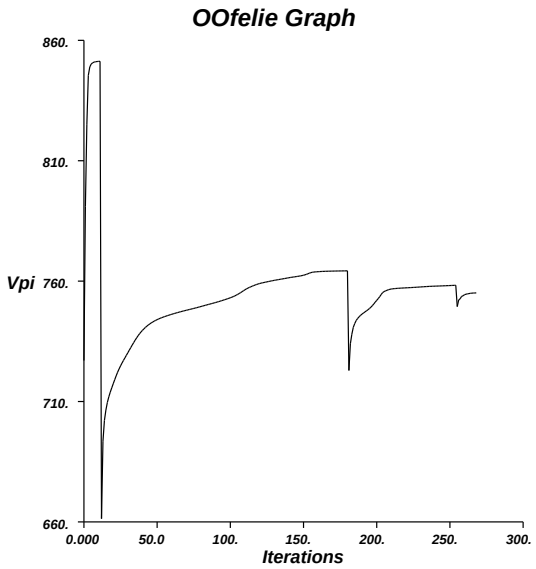

Figure 11: Evolution of the pull-in voltage during optimization process

It turns out form the last result and from physical nature of the pull-in effect that maximizing the pull-in voltage seems to be very similar to maximizing the stiffness of the structure. Therefore one can wonder whether pull-in maximization is not simply equivalent to a linear compliance minimization. In order to investigate the differences between the two optimization problems, the compliance minimization problem has been considered for the same microbeam subjected to a uniform load. Figure 12 presents the compliance optimization results. This figure shows a slightly different topology compared to the previous one. Indeed, we can see that pull-in optimization (see figure 10) tends to place more material (thicker members and more suspension members) in the central part of the domain while compliance optimization is more likely to put material on the sides of the optimization domain. One reason of this difference is that the non-linear analysis considers a stronger loading of the central part of the beam since the deformation makes this portion of the beam closer to the fixed electrode. Values of the objective functions are also different, the final structure pull-in voltage is equal to 722 V that is to say 4.4% less than pull-in optimization while the present structure is 3.3% more efficient in terms of compliance. Therefore, it stems out that the two optimization problems are not strictly equivalent and lead to similar but different results. Nevertheless, this comparison shows that, in the framework of this study, the maximization of the pull-in voltage can be well approximated by a compliance minimization problem. However, if the separation between electrical domain and optimization domain is abandonned, we can expect that the difference between the two approaches will be greater since the electrostatic force distribution is then design dependant.

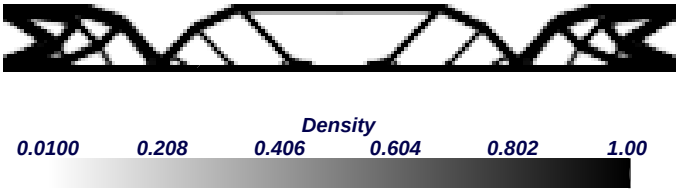

Figure 12: Final topology while optimizing structural compliance

4.2 Microbeam optimization including fabrication constraint

The last application proposes an optimal structure having a lot of closed cavities. These holes make the structure rather complicated to be manufactured using classical MEMS fabrication techniques based on layer deposition. Therefore, on the basis of the previous application, but with a limit volume fraction of 60 %, we have introduced the layer deposition manufacturing constraint in the optimization problem.

However as shown by figure 13, the manufacturing constraint makes the convergence toward a 0-1 material distribution slightly more difficult. This figure shows the result obtained using the same continuation procedure as previously and starting from a uniform distribution. We can see that the optimizer prefers to place intermediate densities in the upper elements of the domain rather than regrouping the material on the electrode. This problem comes probably from the existence of many local optima reinforced by the conservative zero order approximation of the manufacturing constraint. Moreover, the arches created by the optimizer in the first application shows that the elements on the top of the domain possess higher sensitivities than those on the bottom. Therefore, in this application, there exist a strong antagonism between the objective function which tends to increase the density in the upper part of the optimization domain and the manufacturing constraint requiring first an increase of the bottom elements.

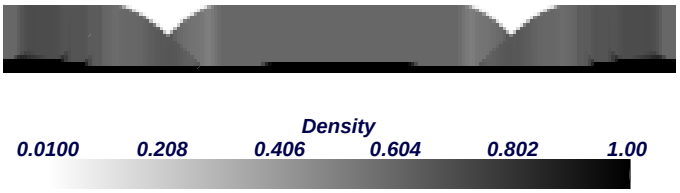

Figure 13: Optimization result for p evolving from 1 to 4 by step of 1

In consequence, the continuation procedure has to be pushed further up. Here we could push this game up to its extreme feasible limit of a non differentiable case with a penalty coefficient equal to 48. The penalty parameter is multiplied by two every 20 iterations. The resulting density distribution is presented in figure 14(a). However, as a high penalty parameter is used here, the density distribution may have no mechanical meaning and it is more meaningful to plot the stiffness distribution. This is done in figure 14(b) where the ratio between the elementary Young Moduli (E) and the full solid Young Modulus (E0) is

plotted. This simple structure makes advantage of the provided supports on the two sides of the optimization domain. Starting from an initial pull-in voltage of 589 V, the objective function is increased by 16% and is finally equal to 686 V. As the same optimization problem without manufacturing constraint leads to an optimal structure similar to the one presented in figure 10 with a pull-in voltage equal to 871 V, the activation of the manufacturing constraint results in a loss of 21% in terms of final pull-in voltage.

(a) Density distribution (b) Stiffness distribution

Figure 14: Optimization result for the clamped-clamped boundary conditions starting from a uniform distribution including manufacturing constraint

However as the process starts from a uniform material distribution, the constraints (13) result in an initial locking of most of the variables. Indeed, at the first iteration, only the first and the last lines can be modified because interior elements are located between two other elements owning the same density. In consequence, the optimization process is quite slow at the beginning.

In order to allow the entire design domain to be modified from the first iteration, another initial distribution has been tested. The idea is to increase linearly the value of the initial density from the top of the design domain to the bottom. The resulting distribution for the current application is presented in figure 15.

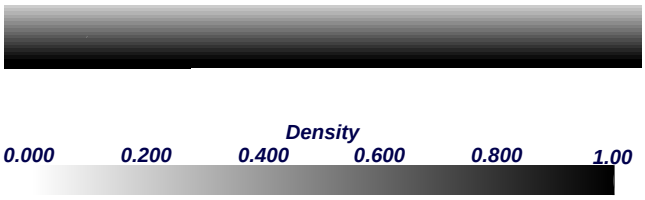

Figure 15: Shaded initial distribution

The modification of the initial distribution has a significant effect on the final structure. Indeed, using a shaded distribution leads to the different solution presented in figures 16 where the density and stiffness maps are presented. The final penalty is the same as with the uniform distribution but in order to obtain consistent results the number of iterations at constant penalty is here reduced to 10. The new structure is slightly more complicated than the previous one, presenting two hinges and looking like the results obtained by Abdalla *et al.* [11] which could be expected since the device behaves almost as a plane capacitor. Therefore we can say that, as here the electrostatic domain is not modified by the optimization process and as the electrostatic force acts mostly vertically, a non-linear plate formulation as the one proposed by Abdalla *et al.* would have been sufficient to model the electrostatic field.

Moreover, the last structure is similar to the one obtained by Seyranian *et al.* for post-buckling optimization of column in reference [34]. The last result indicates that, as often in topology optimization, the pull-in voltage maximization problem possesses several local optima. The final pull-in voltage is lower than when starting from the uniform distribution (643 V).

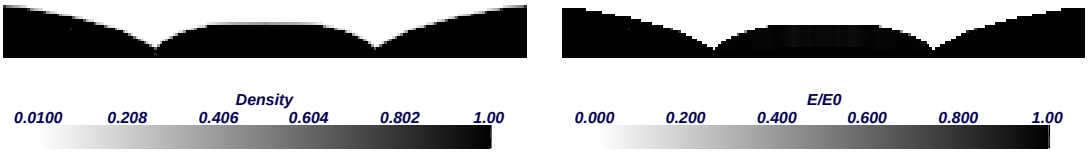

(a) Density distribution (b) Stiffness distribution

Figure 16: Optimization result for the clamped-clamped boundary conditions starting from a shaded distribution including manufacturing constraint

We were interested in determining if the 'one-hinge' solution is always more efficient than the 'two-hinges' solution. We then investigated the optimum over a set of different volume bounds and we observed that this situation can reverse when the maximal volume fraction is increased. Figure 17 summarizes the results obtained for different volume fraction and each starting distribution. The curve markers are related to the initial distribution while the line style (dashed or continuous) indicates the final topology. On this figure, we can verify that for a volume fraction greater than 0.72 the 'two-hinges' topology possesses a higher pull-in voltage than the 'one-hinge'. From a volume fraction of 0.76 the two initial distributions lead to the same topology even if there is still a small difference between optimal pull-in voltages. Below this volume fraction, the two initial distributions give rise to different topologies

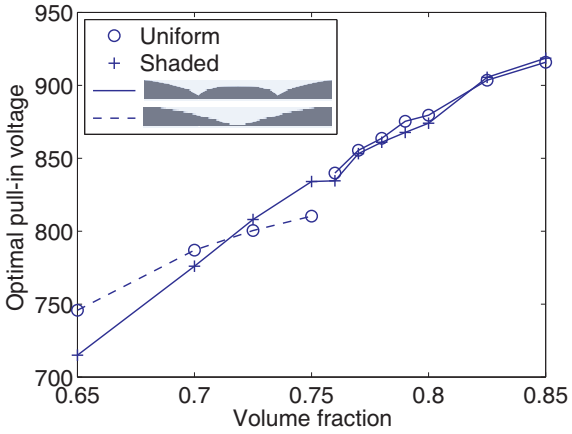

Figure 17: Evolution of the final pull-in voltage with respect to the volume fraction and the starting distribution

The existence of very different local optima reduces the performance of optimized designs. Nevertheless for the considered application, it is possible to deduce design rules, indeed, below a volume fraction equal to 0.72 a 'one-hinge' structure is preferable while for volume fraction

greater than 0.72, the 'two-hinge' bridge is optimal.

From a manufacturing point of view, the presence of hinges in final topologies is not an obstacle. Indeed, hinges can appear in a microstructure as a side effect of the manufacturing process (non-planarized layers in polyMUMPs process [35] for instance). Moreover, they can also be created on purpose with the help of anisotropic or isotropic wet etching techniques (see reference [36]) without increasing a lot the manufacturing process complexity.

5 Conclusion and perspectives

5.1 Conclusion

This paper considers the application of topology optimization to electromechanical devices. One specific aspect of these systems lies in their non-linearity and potentially unstable behavior. Especially, this paper is focused on the pull-in instability of which modeling may be difficult and inaccurate using classical tools. Therefore, we carry out the analysis with the help of a monolithic finite element formulation driven by a normal flow homotopy method.

Within the scope of this preliminary study, we show that it is possible to establish a pull-in voltage topology optimization procedure on the basis of a microbeam optimal reinforcement problem. In this context, an expression of the objective function sensitivities requiring no additional load cases has been developed and validated using a comparison with finite differences. The knowledge of this analytical expression allows us to use efficient mathematical programming optimizers as *CONLIN*.

A numerical application of the developed method is proposed and a comparison with linear compliance optimization is performed. This comparison shows that the compliance optimization is, in the context of the present work, a good approximation of pull-in voltage optimization even if the two objective functions actually lead to different structures. However, this first numerical application has shown that topology optimization creates rather complex geometries on a practical point of view. Indeed, the optimized structures contain a lot of closed cavities, which are difficult to produce using classical MEMS material deposition process.

Consequently, a manufacturing constraint has been introduced in the optimization problem to avoid the creation of closed holes in the structure. The last application have proved the ability of this new constraint to give more realistic results from a fabrication point of view at the cost of a lower pull-in voltage. This application including manufacturing constraint show also that the optimization process experiences difficulties to converge. Indeed, when the manufacturing constraint is activated, strong penalty coefficients have to be used in order to enforce a 0-1 material distribution and the presence of several local optima has been noticed. However, the optimization results allow deducing simple design rules in function of the available material volume. Additionally, the similarities of some results with the ones proposed by Abdalla *et al.* confirms the validity of our approach. Moreover, our more general modeling method will allow us considering more complex optimization problems in the future.

5.2 Future works

Optimization difficulties as local optima encountered while using the manufacturing constraint may find their origin in the implementation of the constraint. Indeed, the use of zero order approximation (i.e. side constraints) is probably too restrictive. In consequence, the

modification of the implementation of the manufacturing constraint is one of the first tasks that will be addressed.

Nevertheless, the present paper shows the possibility to control pull-in voltage in topology optimization. Therefore, we are now able to study more complex optimization problems where pull-in voltage will more likely appear as a constraint. For instance, optimization of electrostatic actuators to maximize displacement of the output point can be considered.

Moreover, stresses are another important feature in MEMS considering the large number of cycles experienced by these devices. The addition of local stress constraints in topology optimization has already been treated by Duysinx and Bendsøe [37]. A similar approach can be used in order to ensure the strength of the device.

Finally, another important goal in our research will be to remove the restriction of the separation between mechanical and electric domain. This step will enlarge the optimization process freedom, allowing the modification of the interface between the physical domains as in Raulli *et al.* [8] and Yoon *et al.* [10]. This modification requires taking into account the electrical effects in the optimization domain and in consequence the modeling of the electrical behavior for intermediate densities. Additionally, it will then be possible to study the design of plane electrodes topology which are often seen in microdevices.

6 Acknowledgments

This research was has been realized under research project ARC 03/08-298 'Modeling, Multiphysics Simulation and Optimization of Coupled Problems - Application to Micro Electro-Mechanical Systems' supported by the Communauté Française de Belgique. The second author acknowledges the financial support of the Belgian National Fund for Scientific Research. Moreover, the authors want to thank Professor C. Fleury for making the *CONLIN* software available.

References

[1] M. Bendsøe, N. Kikuchi, Generating optimal topologies in structural design using a homogenization method, Comput. Methods Appl. Mech. Engrg. 71 (2) (1988) 197–224.

[2] M. Bendsøe, Optimal shape design as a material distribution problem, Struct. Opt. 1 (1989) 193–202.

[3] O. Sigmund, J. Petersson, Numerical instabilities in topology optimization: A survey on procedures dealing with checkerboards, mesh-dependencies and local minima, Struct. Opt. 16 (1) (1998) 68–75.

[4] M. Bendsøe, O. Sigmund, Topology optimization : theory, methods, and applications, Springer Verlag.

[5] S. Wang, J. Kang, Topology optimization of nonlinear magnetostatics, IEEE Transactions on Magnetics 38 (2002) 1029–1032.

[6] O. Sigmund, Design of multiphysic actuators using topology optimization - Part I : One material structures. - Part II : Two-material structures, Comput. Methods Appl. Mech. Engrg. 190 (49–50) (2001) 6577–6627.

[7] L. Yin, G. Ananthasuresh, A novel topology design scheme for the multi-physics problems of electro-thermally actuated compliant micromechanisms, Sens. & Act. 97–98 (2002) 599–609.

[8] M. Raulli, K. Maute, Topology optimization of electrostatically actuated microsystems, Struct. & Mult. Opt. 30 (5) (2005) 342–359.

[9] Z. Liu, J. Korvink, M. Reed, Multiphysics for structural topology optimization, Sensor Letters 4 (2006) 191–199.

[10] G. Yoon, O. Sigmund, Topology optimization for electrostatic system, in: Proceedings of the 7th World Congress on Structural and Multidisciplinary Optimization, 2007, pp. 1686–1693.

[11] M. Abdalla, C. Reddy, W. Faris, Z. Gurdal, Optimal design of an electrostatically actuated microbeam for maximum pull-in voltage, Comp. & Struct. 83 (2005) 1320–1329.

[12] E. Lemaire, P. Duysinx, V. Rochus, J.-C. Golinval, Improvement of pull-in voltage of electromechanical micorbeams using topology optimization, in: III European Conference on Computational Mechanics, 2006.

[13] I. Klapka, A. Cardona, M. Géradin, An object-oriented implementation of the finite element method fro coupled problems, Revue Européenne des Elements Finis 7 (5) (1998) 469–504.

[14] M. Neves, H. Rodrigues, J. Guedes, Generalized topology design of structures with a buckling load criterion, Struct. Opt. 10 (1995) 71–78.

[15] T. Buhl, C. Pedersen, O. Sigmund, Stiffness design of geometrically nonlinear structures using topology optimization, Struct. & Mult. Opt. 19 (2000) 93–104.

[16] S. Rahmatalla, C. Swan, Continuum structural topology optimization of buckling-sensitive structures, AIAA 41 (6) (2003) 1180–1189.

[17] R. Kemmler, A. Lipka, E. Ramm, Large deformation and stability in topology optimization, Struct. & Mult. Opt. 30 (2005) 459–476.

[18] M. Agrawal, G. Ananthasuresh, On including lmanufacturing constraints in the topology optimization of surface-micromachined structures, in: 7th World Congress on Structural and Multidisciplinary Optimization, 2007, pp. 2256–2265.

[19] J. Reitz, F. Milford, R. Christy, Foundations of electromagnetic theory, 3rd Edition, Addison-Wesley, 1979.

[20] W. van Spengen, R. Puers, I. de Wolf, A physical model to predict stictions in mems, Journal of Micromechanics and Microengineering 190.

[21] V. Rochus, D. J. Rixen, J.-C. Golinval, Monolithic modelling of electro-mechanical coupling in micro-structures, Int. J. Numer. Meth. Engng. 65 (4) (2006) 461–493.

[22] M. Géradin, D. Rixen, Mechanical Vibrations : Theory and Application to Structural Dynamics, 2nd Edition, John Wiley & Sons Ltd., 1997.

[23] S. Ragon, Z. Gurdal, L. Watson, A comparison of three algorithms for tracing nonlinear equilibrium paths of structural systems, Int. J. Solids Struct. 39 (2002) 689–698.

[24] M. Crisfield, Non-linear finite element analysis of solids and structures, Wiley, New York, 1991.

[25] A. Seyranian, E. Lund, N. Olhof, Multiple eigenvalues in structural optimization problems, Struct. Opt. 8 (1994) 207–227.

[26] H. A. Eschenauer, N. Olhoff, Topology optimization of continuum structures: A review, Applied Mechanics Reviews 54 (4) (2001) 331–390.

[27] O. Sigmund, On the design of compliant mechanisms using topology optimization, Mech. Struct. Mach. 25 (4) (1997) 493–526.

[28] C. Fleury, Mathematical programming methods for constrained optimization : dual methods, Vol 150 of Progress in astronautics and aeronautics, AIAA chap 7 (1993) 123–150.

[29] K. Svanberg, The method of moving asymptotes - a new method for structural optimization, Int. J. Numer. Meth. Engng. 24 (2) (1987) 359–373.

[30] C. Fleury, Conlin : an efficient dual optimizer based on convex approximation concepts, Struct. & Mult. Opt. 1 (2) (1989) 81–89.

[31] M. Zhou, R. Fleury, Y. Shyy, H. Thomas, J. Brennan, Progress in topology optimization with manufacturing constraints, in: 9th AIAA/ISSMO Symposium on Mutlidisciplinary Analysis and Optimization, AIAA, Atlanta, Georgia, 2002.

[32] M. Zhou, Y. Shyy, H. Thomas, Topology optimization with manufacturing constraints, in: 4th World Congress of Structural and Multidisciplinary Optimization, Dalian, China, 2001.

[33] O. Sigmund, Materials with prescribed constitutive parameters: An inverse homogenization problem, Int. J. Solids Struct. 31 (1994) 2313–2329.

[34] A. Seyranian, O. Privalova, The lagrange problem on an optimal column: old and new results, Struct. Opt. 25 (2003) 393–410.

[35] J. Carter, A. Cowen, B. Hardy, R. Mahadevan, M. Stonefield, S. Wilcenski, PolyMUMPs design hanbook, MEMSCAP, 11th Edition (2005).

[36] S. Senturia, Microsystem Design, Kluwer Academic Publisher, 2001.

[37] P. Duysinx, M. Bendsøe, Topology optimization of continuum structures with local stress constraints, Int. J. Numer. Meth. Engng. 43 (1998) 1453–1478.